Theory of the backward beam displacement on periodically corrugated surfaces and its relation to leaky Scholte-Stoneley waves

Nico F. Declercq[a] and Joris Degrieck
Soete Laboratory, Department of Mechanical Construction and Production, Faculty of Engineering, Ghent University, Sint Pietersnieuwstraat 41, 9000 Gent, Belgium

Rudy Briers
Katholieke Hogeschool Zuid-West Vlaanderen, Department Regentaat en Normaalschool, Sint Jozefstraat 1, 8820 Torhout, Belgium

Oswald Leroy
Interdisciplinary Research Center, KULeuven Campus Kortrijk, E. Sabbelaan 53, 8500 Kortrijk, Belgium

(Received 11 May 2004; accepted 30 August 2004)

A demonstration of the capability of the inhomogeneous wave theory to simulate backward displacement of ultrasonic-bounded beams [M. A. Breazeale and M. Torbett, Appl. Phys. Lett. **29**, 456 (1976)] has been demonstrated recently [N. F. Declercq, J. Degrieck, R. Briers, and O. Leroy, Appl. Phys. Lett. **82**, 2533 (2003)]. The current report applies the theory of the diffraction of inhomogeneous waves and shows how this theory is capable of simulating, explaining, and understanding the experiments mentioned above. The theory reveals the existence of leaky Scholte-Stoneley waves, a phenomenon suggested theoretically [N. F. Declercq, J. Degrieck, R. Briers, and O. Leroy, J. Acoust. Soc. Am. **112**, 2414 (2002)] and observed experimentally [A. A. Teklu, M. A. Breazeale, J. Acoust. Soc. Am. **113**, 2283 (2003)]. Moreover, the present paper shows that the classical Fourier decomposition of bounded beams is unable to simulate the backward beam displacement. This work also elucidates the nature of Wood anomalies in Diffraction spectra. © *2004 American Institute of Physics*. [DOI: 10.1063/1.1808247]

I. INTRODUCTION

There are several ways to tackle the diffraction of sound by a periodically corrugated surface.[1] The method applied here is the one that is based on the "Rayleigh decomposition" of the diffracted sound field into single bulk inhomogeneous waves, all traveling in directions, determined by the classical grating equation. The validity of this approach has been proved by Briers,[2] and Briers *et al.*.[3] In fact, it is an inhomogeneous wave extension of the more classical approach that can be found in Claeys and Leroy[4] and Claeys *et al.*,[5] where the generation of diffracted plane waves is assumed. The validity of the latter method, where a decomposition into plane waves is used, is shown by Lippmann,[6] who states that it is correct whenever the incident wavelength is of the same order of magnitude as the corrugation period and the height of the corrugation is small compared to it. Claeys and Leroy[4] and Claeys *et al.*[5] studied the diffraction of plane waves on periodically corrugated liquid-solid interfaces, and Jungman *et al.*,[7] Mampaert and Leroy,[8] Mampaert *et al.*,[9] and Declercq *et al.*[10] studied this phenomenon on periodically corrugated solid-liquid interfaces. The latter showed that the diffraction of plane waves can be used to simulate the appearance of the so-called Wood anomalies[5] in diffraction spectra for normal incident sound. Wood anomalies are strong amplitude dips in the reflection spectra and are caused by energy transformation of incident sound into the Scholte-Stoneley waves. Briers,[2] Briers *et al.*,[3] Deschamps and Cheng,[11] and Briers and Leroy[12,13] extended the theory of the diffraction of homogeneous plane waves to that of inhomogeneous plane waves and experimentally proved the validity of their approach. They also studied the diffraction on periodically corrugated solid plates immersed in water.[2] Besides the success of the mentioned papers, there remains the obscurity of the exact nature of Wood anomalies[5] and the explanation of what really happens in the experiments of Breazeale and Torbett[14] that show the appearance of a backward beam displacement on periodically corrugated surfaces. The present work explains the experiments of Breazeale and Torbett[14] by applying the theory of the diffraction of inhomogeneous plane waves, properly involving some considerations of Deschamps,[15] and gives a comprehensive explanation of the nature of the Wood anomalies in diffraction spectra.

II. THE EXPERIMENT OF MACK BREAZEALE AND MICHAEL TORBETT[14]

Breazeale and Torbett[14] have performed experiments that originally were intended to verify the prediction of Tamir and Bertoni,[16] that, similar to their counterpart in optics, backward-traveling acoustic surface waves, originating from diffraction, would cause a backward acoustical beamshift of the reflected sound. Breazeale and Torbett[14] let a bounded sound beam impinge from the liquid side, onto a periodically corrugated interface between water and brass. According to the classical diffraction equation, a backward-traveling first-order lateral wave (for example, a lateral bulk wave, a Scholte-Stoneley wave, or a leaky Rayleigh wave) exists if

[a]Electronic mail: NicoF.Declercq@ugent.be

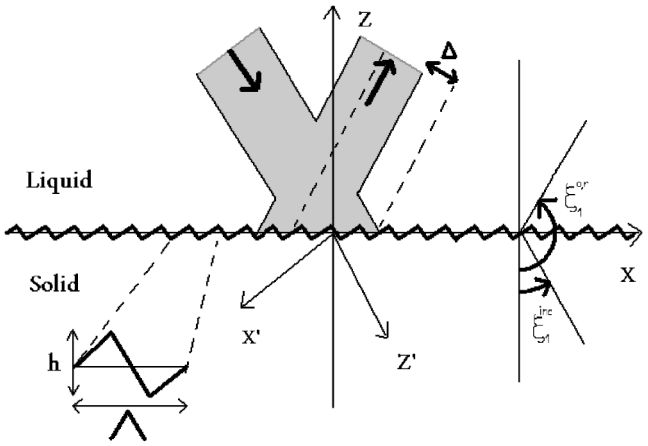

FIG. 1. Diagram of the backward beam displacement Δ on a periodically corrugated surface with period Λ and height *h*.

sound is incident from a real angle ξ^{inc} (*inc* stands for incident) with[14]

$$\sin \xi^{inc} = \nu_l \left(\frac{1}{f\Lambda} - \frac{1}{\nu_{BT}} \right), \tag{1}$$

in which ν_l is the sound velocity in the covering liquid, f is the frequency, Λ is the corrugation period, and ν_{BT} is the velocity of the lateral wave. If the velocity of the leaky Rayleigh waves (2015 m/s) on a smooth water-brass interface is entered in (1), at a frequency of 6 MHz, one finds an angle of incidence of 41°. This stimulated Breazeale and Torbett[14] to seek for a backward beamshift around 41°. The result was negative. Furthermore, they looked at other angles of incidence and found the backward beamshift in the vicinity of 22.5°, which led them to the primary conclusion that if the effect was caused by a backward-traveling lateral wave, it would have a velocity ν_{BT}=1470 m/s, which differs quite a lot from the Rayleigh velocity. They concluded that more experimental and theoretical research was necessary to determine what really was the cause of this backward beamshift. Moreover, if they kept that particular angle of incidence and changed the frequency to 2 MHz, the backward beamshift was not there anymore. In what follows, the inhomogeneous waves theory will show us that it is not a simple expression as (1) that determines the effect, but a complicated interaction between all diffracted orders. The next section treats the theoretical description of the interaction of one single inhomogeneous wave. Further, such single inhomogeneous waves will be superposed to form a bounded beam that interacts with the periodically corrugated surface under consideration.

III. THE DIFFRACTION OF INHOMOGENEOUS WAVES

A. Description of the incident and the diffracted wave field

Consider a periodically corrugated interface between a liquid and a solid as depicted in Fig. 1. The corrugation is periodic with period Λ and is given by

$$z = f(x) \tag{2}$$

with

$$f(x+\Lambda) = f(x). \tag{3}$$

It is convenient to write (2) as

$$g(x,z) = f(x) - z = 0. \tag{4}$$

Taking into account the Rayleigh decomposition of the diffracted wave field and taking into account characteristics of dilatational and shear waves, the displacement of the incident waves N^{inc}, the (dilatational) reflected waves N^r, and the dilatational and shear waves in the solid N^d and N^s, respectively, may be written as

$$N^{inc} = A^{inc}\varphi^{inc}(ik_x^{inc}e_x + ik_z^{inc}e_z), \tag{5}$$

with

$$N^r = \sum_m A_m^r \varphi^{m,r}(ik_x^{m,r}e_x + ik_z^{m,r}e_z), \tag{6}$$

$$N^d = \sum_m A_m^d \varphi^{m,d}(ik_x^{m,d}e_x + ik_z^{m,d}e_z), \tag{7}$$

$$N^s = \sum_m A_m^s P^{m,s} \varphi^{m,s}, \tag{8}$$

with

$$\varphi^{\varsigma} = e^{i(k^{\varsigma}\cdot r)} \tag{9}$$

and

$$k_x^{m,s}P_x^{m,s} + k_y^{m,s}P_y^{m,s} + k_z^{m,s}P_z^{m,s} = 0. \tag{10}$$

In relations (5)–(10), A stands for the amplitude, P stands for the polarization vector, whereas the index m denotes the diffraction order, and ς represents *inc*, m,r, m,d, or m,s.

The following properties that hold for inhomogeneous waves[17] also need to be taken into account:

$$k^{\varsigma} = k_1^{\varsigma} + ik_2^{\varsigma}, \tag{11}$$

$$k_2^{\varsigma} = \alpha^{\varsigma} - \beta^{\varsigma}, \tag{12}$$

$$k_1^{\varsigma} \cdot k_2^{\varsigma} = k_1^{\varsigma}\alpha^{\varsigma}, \tag{13}$$

$$\beta^{\varsigma} \perp k_1^{\varsigma}, \tag{14}$$

$$\alpha^{\varsigma} | k_1^{\varsigma}, \tag{15}$$

$$(k_1^{\varsigma})^2 - (\alpha^{\varsigma})^2 - (\beta^{\varsigma})^2 = \left(\frac{\omega}{\nu_{\varsigma}}\right)^2 - (\alpha_0^{\varsigma})^2, \tag{16}$$

with ν_{ς} as the sound velocity and α_0^{ς} as the intrinsic damping coefficient. The vector α^{ς} is called the damping vector, while the vector β^{ς} is called the inhomogeneity vector.

B. The continuity conditions

The incident wave is described by the amplitude A^{inc}, the real part k_1^{inc}, and imaginary part k_2^{inc} of the wave vector and incidence angle ξ_1^{inc}, so that, for nonabsorbing media

$$
\begin{aligned}
k_{1,x}^{inc} &= k_1^{inc} \sin \xi_1^{inc},\\
k_{1,z}^{inc} &= -k_1^{inc} \cos \xi_1^{inc},\\
k_{2,x}^{inc} &= k_2^{inc} \sin \xi_2^{inc},\\
k_{2,z}^{inc} &= -k_2^{inc} \cos \xi_2^{inc},
\end{aligned}
\tag{17}
$$

with

$$
\xi_2^{inc} = \xi_1^{inc} - \pi/2.
$$

The signs in (17) are chosen to fulfill the definitions of the angles and axes in Fig. 1. In media τ ($\tau=1$ in the liquid and $\tau=2$ in the solid), the stress tensor T^{τ} is given[11,18] by its elements

$$
T_{ij}^{\varsigma} = \sum_{\eta} \left(\lambda_1^{\tau} + \lambda_2^{\tau}\frac{\partial}{\partial t}\right)\varepsilon_{\eta\eta}^{\tau}\delta_{i,j} + 2\left(\mu_1^{\tau} + \mu_2^{\tau}\frac{\partial}{\partial t}\right)\varepsilon_{i,j}^{\tau}, \tag{18}
$$

in which the strain tensor ε_{ij}^{τ} is

$$
\varepsilon_{ij}^{\tau} = \frac{1}{2}[\partial_i N_j^{\tau} + \partial_j N_i^{\tau}]. \tag{19}
$$

The Lamé constants are denoted by λ_1^{τ} and μ_1^{τ}, while the viscosity coefficients are given by λ_2^{τ} and μ_2^{τ}. They obey the dispersion relations[17] (13) and (16) if

$$
k^{\varsigma}\cdot k^{\varsigma} = \frac{\rho\omega^2}{(\lambda_1^{\tau} - i\omega\lambda_2^{\tau}) + 2(\mu_1^{\tau} - i\omega\mu_2^{\tau})} \tag{20}
$$

for the dilatational waves ($\varsigma = inc$ or m,r) in the liquid and ($\varsigma = m,d$ or m,s) in the solid, and if

$$
k^{\varsigma}\cdot k^{\varsigma} = \frac{\rho\omega^2}{(\mu_1^{\tau} - i\omega\mu_2^{\tau})} \tag{21}
$$

for shear waves ($\varsigma = s,2$) in the solid. The Lamé constants are related to the shear velocity ν_s^{τ}, the dilatational velocity ν_d^{τ}, the intrinsic damping coefficient for shear waves $\alpha_{s,0}^{\tau}$, and the intrinsic damping coefficient for dilatational waves $\alpha_{d,0}^{\tau}$ through the dispersion relations (13) and (16).

In order to find the unknown coefficients $A_m^r, A_m^d, A_m^s P_x^{m,s}, A_m^s P_y^{m,s}$, and $A_m^s P_z^{m,s}$, the equations that describe the continuity of normal stress and strain along the interface (4) must be solved, i.e.,

$$
(N^{inc} + N^r)\cdot\nabla g = (N^d + N^s)\cdot\nabla g \text{ along } g = 0, \tag{22}
$$

$$
\sum_j T_{ij}^1(\nabla g)_j = \sum_j T_{ij}^2(\nabla g)_j \text{ along } g = 0, \tag{23}
$$

and also [see (10)]

$$
(A_m^s P_x^{m,s} k_x^{m,s} + A_m^s P_y^{m,s} k_y^{m,s} + A_m^s P_z^{m,s} k_z^{m,s})\varphi^{m,s} = 0. \tag{24}
$$

Conditions (22)–(24) lead to five equations that are periodic in x, whence a sufficient condition for a correct solution is that the Fourier coefficients (for a discrete Fourier transform over the interval $[0\rightarrow\Lambda]$) are equal. The wave vectors that are introduced by this discrete Fourier transform are denoted by the order p.

The five equations for each integer p are Equation (1)

$$
\begin{aligned}
&A^{inc} I^{inc,p} i(-(k^1)^2 + k_x^{inc} k_{x,p}) + \sum_m A_m^r I^{m,r,p} i(-(k^1)^2 + k_x^m k_x^p)\\
&\quad + \sum_m A_m^d I^{m,d,p} i((k^{d,2})^2 - k_x^m k_x^p) - \sum_m A_m^s P_x^{m,s} I^{m,s,p}(k_x^p\\
&\quad - k_x^m)\\
&\quad + \sum_m A_m^s P_z^{m,s} I^{m,s,p}(k_z^{m,s}) = 0,
\end{aligned}
\tag{25}
$$

Equation (2)

$$
\begin{aligned}
&-A^{inc} I^{inc,p}\rho_1(k_x^p - k_x^{inc}) - \sum_m A_m^r I^{m,r,p}\rho_1(k_x^p - k_x^m)\\
&\quad + \sum_m A_m^d I^{m,d,p}\rho_2\left(-k_x^m + \left(1 + 2\frac{(k_x^m)^2 - (k^{d,2})^2}{(k^{s,2})^2}\right)k_x^p\right)\\
&\quad + \sum_m A_m^s P_x^{m,s} I^{m,s,p} i\rho_2\left(1 - \frac{k_x^m k_x^p}{(k^{d,2})^2} + \left(\frac{1}{(k^{d,2})^2} - \frac{1}{(k^{s,2})^2}\right)\right.\\
&\quad \left.\times(k_x^m)^2\right) + \sum_m A_m^s P_z^{m,s} I^{m,s,p}\rho_2 i(k_z^{m,s})\left(\left(\frac{1}{(k^{d,2})^2}\right.\right.\\
&\quad \left.\left. - \frac{1}{(k^{s,2})^2}\right)k_x^m - \left(\frac{1}{(k^{d,2})^2} - \frac{2}{(k^{s,2})^2}\right)k_x^p\right) = 0,
\end{aligned}
\tag{26}
$$

Equation (3)

$$
+\sum_m A_m^s P_y^{m,s} I^{m,s,p} i\rho_2\left(1 - \frac{k_x^m k_x^p}{(k^{s,2})^2}\right) = 0, \tag{27}
$$

Equation (4)

$$
\begin{aligned}
&+A^{inc} I^{inc,p}\rho_1(k_z^{inc})^2 e^{-ik_z^{inc} z_0}\\
&\quad + \sum_m A_m^r I^{m,r,p}(k_z^{m,r})\rho_1\\
&\quad + \sum_m A_m^d I^{m,d,p}(k_z^{m,d})\rho_2\left(-1 + \frac{2}{(k^{s,2})^2}(k_x^m k_x^p)\right)\\
&\quad + \sum_m A_m^s P_x^{m,s} I^{m,s,p} i(k_z^{m,s})\rho_2\left(\left(\frac{1}{(k^{d,2})^2} - \frac{1}{(k^{s,2})^2}\right)k_x^m\right.\\
&\quad \left. - \frac{k_x^p}{(k^{s,2})^2}\right) + \sum_m A_m^s P_z^{m,s} I^{m,s,p} i\rho_2\left(\left(\frac{1}{(k^{d,2})^2} - \frac{1}{(k^{s,2})^2}\right)\right.\\
&\quad \left.\times(k_z^{m,s})^2 + 1 - \frac{k_x^m k_x^p}{(k^{s,2})^2}\right) = 0,
\end{aligned}
\tag{28}
$$

Equation (5) for $\delta_{m,p}$ Kronecker's delta

$$
(A_m^s P_x^{m,s} k_x^{m,s} + A_m^s P_y^{m,s} k_y^{m,s} + A_m^s P_z^{m,s} k_z^{m,s})\,\delta_{m,p} = 0, \tag{29}
$$

with $(k^1)^2$ and $(k^{d,2})^2$ given by (20) and $(k^{s,2})^2$ given by (21), and with the grating equation[3]

$$
k_x^m = k_x^{inc} + m\frac{2\pi}{\Lambda} \tag{30}
$$

(an equivalent expression holds of course for k_x^p) and

$$
I^{inc,\eta} = \frac{1}{k_z^{inc}}\int_{\Lambda} e^{i(k_x^{inc} - k_x^{\eta})x} e^{i(k_z^{inc} f(x))} dx, \tag{31}
$$

$$I^{m,\xi,\eta} = \frac{1}{k_z^{m,\xi}} \int_{\Lambda} e^{i[(k_x^m - k_x^\eta)x + k_z^{m,\xi} f(x)]} dx. \tag{32}$$

It is already seen from (27) that

$$A_m^s P_y^{m,s} = 0. \tag{33}$$

C. Consideration of Deschamps' rule

A mode m,q inside the solid ($q=s$ or $q=d$), is accompanied by a reflected companion m,r. The angle of propagation of the considered mode m,q is

$$|\xi_1^{m,q}| = \arctan\left[\frac{|k_{1,x}^m|}{|k_{1,z}^{m,q}|}\right]. \tag{34}$$

Whereas the angle of propagation of the reflected companion is

$$|\xi_1^{m,r}| = \arctan\left[\frac{|k_{1,x}^m|}{|k_{1,z}^{m,r}|}\right], \tag{35}$$

From Deschamps,[15] we learn that each diffracted wave must travel away from the interface. However, if $\mathrm{Re}(k_z)=k_{1,z}\neq 0$, then the sign of k_z for the considered mode m,q depends on the angle of propagation of the liquid-side companion, denoted by m,r. If the considered mode m,q inside the solid ($q=s$ or $q=d$) is "close enough" to $\pi/2$, then that particular mode m,q must show the leaky Rayleigh wave features, whence the inhomogeneity vector must point into the liquid. Close enough to $\pi/2$ means that the liquid-side companion must fulfill

$$|\xi_1^{m,r}| > \left|\arcsin\left(\frac{\nu_l}{\nu_q}\right)\right|, \tag{36}$$

where ν_l is the wave velocity in the liquid and ν_q is the wave velocity of the considered mode q,m. Whenever

$$|\xi_1^{m,r}| \leqslant \left|\arcsin\left(\frac{\nu_l}{\nu_q}\right)\right|, \tag{37}$$

Deschamps' rule doesn't need to be considered, whence the Sommerfeld conditions hold, demanding that the mode q,m travels away from the interface.

D. Truncation of infinite summations

The linear set of Eqs. (25)–(29) is infinite, because m,p may take every possible integer value for $-\infty \rightarrow +\infty$. However, it has been shown[4,9,10] that the interval of integers may be truncated to $\{-N,-N+1,\ldots N-1,N\}$ for N larger than 6.

From Refs. 19 and 20, it is known that for a sawtooth profile

$$f(x) = \frac{2hx}{\Lambda} - \frac{h}{2} \text{ if } 0 \leqslant x < \frac{\Lambda}{2}, \tag{38}$$

$$f(x) = \frac{3h}{2} - \frac{2hx}{\Lambda} \text{ if } \frac{\Lambda}{2} \leqslant x < \Lambda, \tag{39}$$

the integrals (31) and (32) become

$$I^{inc,\eta} = ih\Lambda e^{-ihk_z^{inc}/2} \frac{1-(-1)^{-\eta} e^{ihk_z^{inc}}}{(hk_z^{inc})^2 - (\pi\eta)^2}, \tag{40}$$

$$I^{m,\eta,\xi} = ih\Lambda e^{-ihk_z^{inc}/2} \frac{1-(-1)^{(m-\eta)} e^{ihk_z^{m,\xi}}}{(hk_z^{m,\xi})^2 - \pi^2(m-\eta)^2}. \tag{41}$$

In this work, only sawtooth profiles (38) and (39) have been taken under consideration.

IV. THE DIFFRACTION OF A BOUNDED BEAM

A. Description of bounded beams

The Fourier decomposition is described in Ref. 10. It has been shown by Leroy and co-workers that the description of bounded beams by the Fourier decomposition leads to contradictions, such as waves considered incident at angles exceeding 90°. Leroy and co-workers showed that this decomposition was not sufficiently appropriate to describe and to understand what happens if bounded beams are incident at critical angles such as the Rayleigh angle.

The concept of using inhomogeneous waves to decompose a bounded beam was introduced by Claeys[20] and Claeys and Leroy,[22] and is based on the mathematical fact that a smooth beam profile can be locally approached by a summation of exponential functions.[24] This leads to the perception that a bounded beam can be decomposed in a series of inhomogeneous waves, all traveling in the same direction but having different amplitudes and inhomogeneities. Therefore,

$$\Omega(x',z') = \sum_{n=-\infty}^{n=+\infty} B(n,c) e^{-\beta^n x'} e^{ik_z^{n'}(z'-c)}. \tag{42}$$

B. The description of the zero-order reflected beam

Each of the individual waves in the decomposition (42) is diffracted into an infinite number of diffraction orders, whence the reflected sound field is

$$\Xi(x,z) = \sum_{n=-N}^{n=+N} B(n,c) R_0 \gamma_0(x,z) + \sum_{n=-N}^{n=+N} B(n,c) \sum_{m=-\infty}^{m=+\infty} (1 - \delta_{n,0}) R_m \gamma_m(x,z), \tag{43}$$

in which R_m is the reflection coefficient of diffraction order m, and γ_m is the wave function of diffraction order m (i.e., a plane wave or an inhomogeneous wave).

We call

$$\Xi_0(x,z) = \sum_{n=-N}^{n=+N} B(n,c) R_0 \gamma_0(x,z) \tag{44}$$

as the zero-order reflected beam. It is this beam that is called "reflected beam."

V. DISCUSSION OF NUMERICAL RESULTS

A. What really causes Wood anomalies in diffraction spectra?

In the articles of Claeys *et al.*,[5] Mampaert and co-workers,[7–9] and Declercq *et al.*,[10] one deals with the diffraction of pure plane waves on periodically corrugated surfaces. It is seen there that diffraction spectra for normal incidence show the Wood anomalies at certain frequencies. These anomalies are believed to originate from the generation of the Scholte-Stoneley waves. In what follows, we show that Wood anomalies originate from the resonant interaction between forward and backward-traveling Scholte-Stoneley waves.

If one reconsiders the grating Eq. (30), and if one writes any of the diffraction displacements as

$$N^{s} = \sum_{m=-M}^{m=M} A_m^{s} \exp[i(k_x^{m,s}x + k_z^{m,s}z)] \tag{45}$$

with

$$A_m^{s} = (A_{m,x}^{s}e_x + A_{m,y}^{s}e_y + A_{m,z}^{s}e_z), \tag{46}$$

then, for normal incidence,

$$N^{s} = \sum_{m=1}^{m=M} \left[2A_m^{s} \cos\left(\frac{2\pi m}{\Lambda}x\right)\right] \exp(ik_z^{m,s}z) + A_0^{s} \exp\left[i\left(\frac{\omega}{v^{s}}z\right)\right]. \tag{47}$$

If the frequency and the material parameters are such that for a certain diffraction order m, a Scholte-Stoneley wave is stimulated, then one of the diffraction order m^{-} also is stimulated and both interact to create a standing wave phenomenon, whose wavelength λ^{s} fits an integer number of times into one corrugation wavelength Λ [see (47)]. In other words, the superposition of the backward- and forward-traveling Scholte-Stoneley waves cause a vibration eigenstate of the corrugated surface. This eigenstate is the actual reason why under these circumstances, almost all of the incident energy is absorbed by the surface, resulting in the observation of a Wood anomaly in the diffraction spectra.

For oblique incidence, relation (47) does not hold, whence the generation of a Scholte-Stoneley wave does not cause an eigenstate. The absence of an eigenstate diminishes the effect of the generated Scholte-Stoneley wave on the reflected sound intensity, as seen in Fig. 4 of Ref. 25. A more precise explanation is the fact that the Scholte-Stoneley wave of a particular diffraction order, traveling in one direction, is disturbed by the bulk wave of the opposite diffraction order.

The same reasoning holds for the leaky Rayleigh waves if inhomogeneous incident waves are considered. Briers[2] and Briers *et al.*[3,26] showed that, normally, incident inhomogeneous waves under the correct circumstances may induce pure leaky Rayleigh waves, having the same amplitude distribution as for the leaky Rayleigh waves on smooth interfaces. It is expected that for oblique incidence, a generated Rayleigh wave is disturbed by diffraction orders.

TABLE I. The physical properties of water and brass used in our calculations.

	Water	Brass
Density kg/m^3	1000	8100
Longitudinal wave velocity [m/s]	1480	4840
Shear wave velocity [m/s]	0	2270

B. Results and discussion of the reflection coefficients for single inhomogeneous waves incident where Breazeale and Torbett[14] observed a backward displacement

The calculations that have been performed here make use Eqs. (25)–(29) taking into account (38)–(41) for orders ranging from −8 to +8. This results in a matrix equation where all the amplitudes of the diffracted wave orders are found at once. Zero-order reflected waves travel along the specular direction. Other orders travel in directions governed by (30) and (34) together with the dispersion relations (20) and (21). Numerical results are presented for oblique incidence of inhomogeneous waves of 6 MHz on a periodically sawtooth corrugated water-brass interface. The physical properties of water and brass listed in Table I are applied. In consistency with Breazeale and Torbett,[14] a corrugation period $\Lambda = 178$ μm and a corrugation height $h = 25$ μm is used.

In Fig. 2 (top), the magnitude in decibel, viewed from above, of the zero-order reflection coefficient is depicted near the angle where, in Ref. 14, a backward beamshift is found. It is seen that an amplitude dip appears at an angle of incidence of 22.59° and inhomogeneity of −71.86 m^{-1}. This means that the corresponding zero-order reflected inhomogeneous wave is backwards displaced relatively to its incident companion. That this effect also appears for bounded beams,

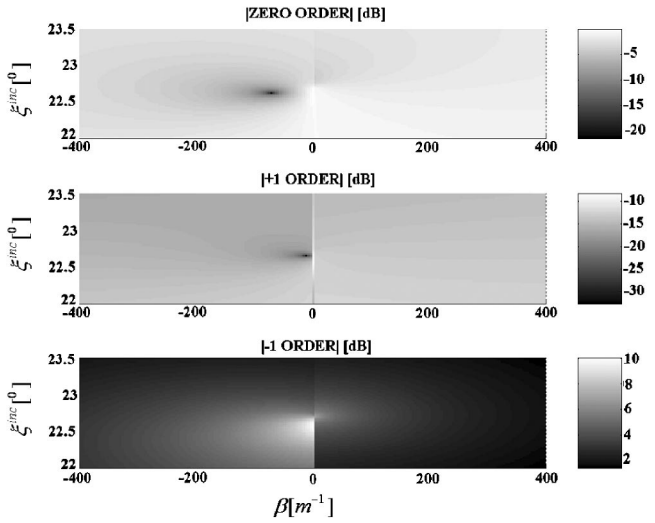

FIG. 2. Magnitude in decibel of the zero-order reflection coefficient (top), as a function of the angle of incidence and the incident inhomogeneity "beta," shows a dip at 22.59° and inhomogeneity of −71.86 m^{-1}. The one for the −1-order reflection coefficient (middle) shows a maximum (not a pole) at 22.56° and inhomogeneity of approximately −1 m^{-1}. The one for the +1-order reflection coefficient (bottom) shows fluctuations, even though the amplitude is overall rather small.

is described below, where results are shown for bounded beams. Figure 2 (middle) shows that the conditions, at which the dip is there in Fig. 2 (top), do not correspond to a strong maximum of the −1-order reflection coefficient, see Fig. 2 (bottom). In fact, the actual maximum is situated very close to but not at $\beta^{inc}=0$, at an angle of incidence of 22.56°. In addition, a strong maximum observed in the −1 order corresponds to the generation of the leaky Scholte-Stoneley waves. First, under the assumption that it is a surface wave, the velocity corresponding to this angle of incidence reveals a velocity of 1477 m/s, which is lower than the velocity of plane waves in water, and which is reasonable for the Scholte-Stoneley waves. Second, the maximum is close to $\beta^{inc}=0$ but is not equal to it. If we compare with the discussion of the Wood anomalies in the previous section, we can come to the following interpretation: The Scholte-Stoneley wave is not much stimulated at $\beta^{inc}=0$ due to the oblique incidence. Stronger stimulation occurs if the incident wave contains already some negative inhomogeneity (by which a higher amplitude is situated closer to the interface than if pure plane waves were incident) and results in a leaky feature of the excited scholte-Stoneley wave. This is the reason for $\beta^{inc}\approx 1$; a maximum is observed in the −1 reflection coefficient. Still, it remains a limited maximum, not a pole. Briers[2] showed that, due to the grating Eq. (30), only pure plane waves are capable of stimulating (nonleaky) Scholte-Stoneley waves.

If one needs to understand what causes the amplitude dip in the zero-order reflection coefficient, one must not only take into account this leaky Scholte-Stoneley wave, but also sound stimulated by additional diffraction orders.

It is seen that the amplitude of the +1-order reflected wave nowhere exceeds unity. However, it also seems to be stimulated more or less depending on the angle and inhomogeneity of incidence. It is the interaction of the −1 order with that of the +1 order that determines what happens with the zero-order reflection coefficient. The same conclusion holds for higher-order diffracted waves, even though their influence is more negligible.

C. Results and discussion of the reflection coefficients for single inhomogeneous waves incident near the expected Rayleigh angle

In Fig. 3, we present the results in decibel, viewed from above. It is seen that the area between 42° and 47° contains a distribution of peaks and dips of the zero-order reflection coefficient at inhomogeneities that are much larger than in the case of Fig. 2. It is important to notice that a peak (or a valley) in the zero-order reflection coefficient for negative (or positive) inhomogeneities causes a shift to the right and a valley (or a peak) in the zero-order reflection coefficient for positive (or negative) inhomogeneities causes a shift to the left. Therefore, two peaks or two valleys at symmetrical positions relative to the axis of the angle of incidence, thwart each others effect in a bounded beam. (This situation appears more or less in Fig. 3.) A peak and a valley at symmetrical positions relative to the axis of the angle of incidence causes a strong cooperation in shifting waves to the left or to the right. (This situation appears more or less in Fig. 2.)

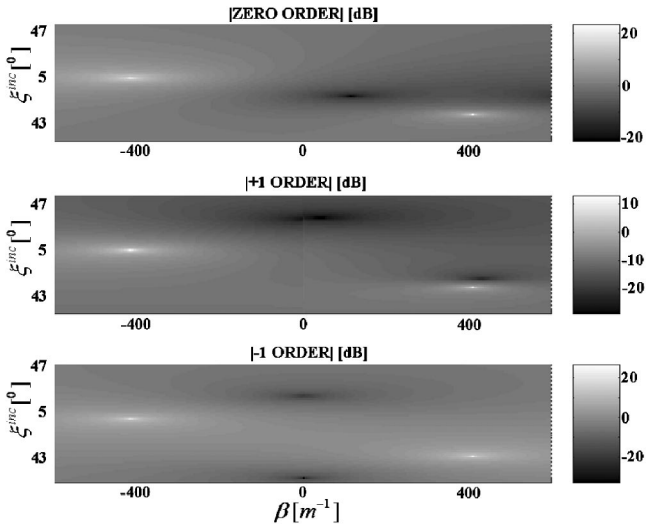

FIG. 3. Amplitude in decibel of the 0-order, 1-order, and −1-order reflection coefficients as a function of the angle of incidence and the incident inhomogeneity. Peaks and valleys appear for larger inhomogeneities than in Fig. 2.

D. Results and discussion of particle displacement fields near the angle where Breazeale and Torbett[14] observed a backward beamshift

Figure 4 shows the displacement for the total diffraction field under the conditions that correspond to the dip in Fig. 2 (top). This field is much different than the field that would be expected if a pure Scholte-Stoneley wave was depicted. However, this is due to the fact that it is formed by the interaction of a leaky Scholte-Stoneley wave and the other diffraction orders (as discussed above). Its propagation is shown in Figs. 5 and 6. What is really interesting in Fig. 4 is the fact that it shows an equivalent pattern, as the one for the leaky Rayleigh waves. In other words, the complete diffraction field that corresponds to the dip in Fig. 2 shows the same amplitude pattern (not the exact values of course) as that corresponding to the leaky Rayleigh wave peak in Fig. 3 at $\theta^{inc}=44.64°$ and $\beta^{inc}=-419.0\ \mathrm{m}^{-1}$ if in the latter, only the

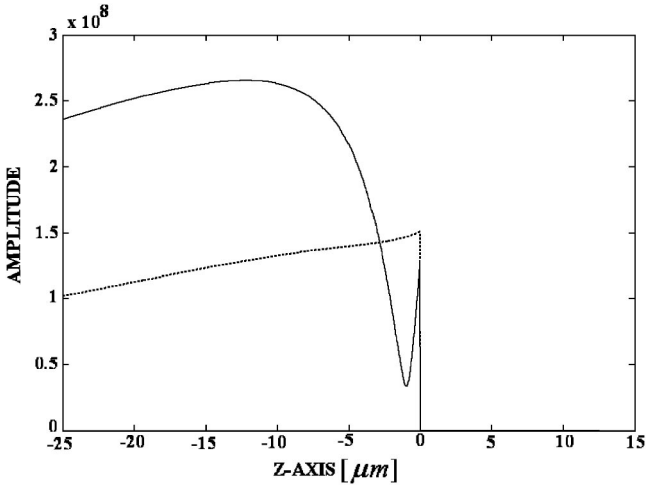

FIG. 4. Amplitude of the complete particle displacement field as a function of depth (negative z values in the solid, positive z values in the liquid) for $\theta^{inc}=22.59°$, $\beta^{inc}=-71.86\ \mathrm{m}^{-1}$, and a frequency of 6 MHz. Solid line: x displacement, dotted line: z displacement. The pattern shows some resemblance with the typical pattern of the Rayleigh waves.

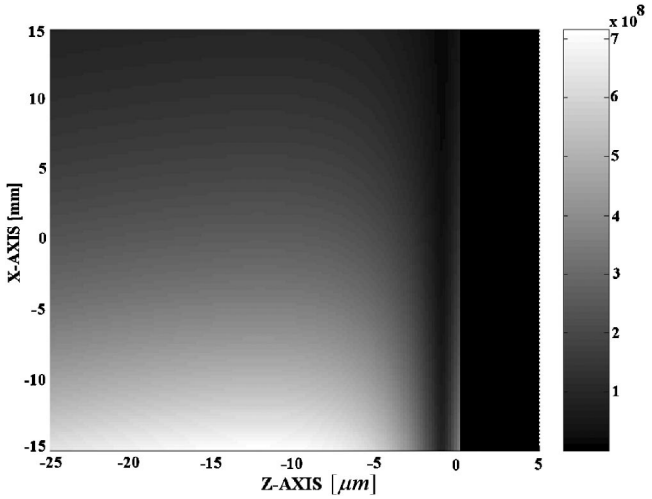

FIG. 5. Amplitude of the *x* displacement as a function of depth and propagation. Same physical circumstances as in Fig. 4. Due to energy leakage, the amplitude drops while propagating.

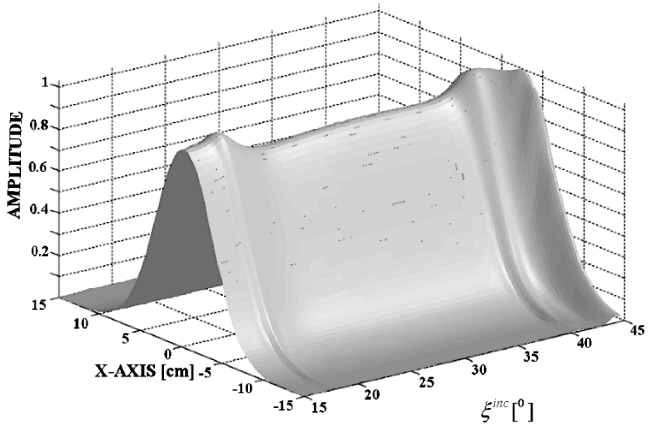

FIG. 7. Reflected beam profile as a function of the angle of incidence at a frequency of 6 MHz. The Fourier method is used. The physical beamwidth is approximately 10 cm. No explicit beam displacement is observable. There is some effect at 17.80°, which is due to the critical angle for dilatational lateral bulk waves, and also at 40.69°, which is due to the critical angle for shear lateral bulk waves.

particle displacement field, due to waves traveling in the direction of the Rayleigh wave, are considered. We have no explanation for this, except perhaps that the combination of the leaky Scholte-Stoneley wave, together with the other diffracted orders, generate a wave field similar to a leaky Rayleigh wave, though having a different velocity.

E. Results for bounded beams using the Fourier decomposition

If a bounded beam, described as a superposition of plane waves, would fully explain what Breazeale and Torbett[14] observed experimentally, then the more elaborate study using inhomogeneous waves would be unnecessary. In Figs. 7 and 8, the reflected beam pattern at 6 MHz is shown as a function of the angle of incidence, using the Fourier method. Figure 7 shows that for a very wide beam (approximately 10 cm physical width), there is no really any significant beamshift observable, except for some small disturbance at bulk critical angles. If, however, a physical beamwidth of approximately 1 cm is used (Fig. 8), which corresponds to the beamwidth in the experiments of Breazeale and Torbett,[14] significant beam deformations and beamshifts appear between 35° and 45°. The latter have not been observed experimentally. There is also nothing significant observable in Fig. 8, near the angle where Breazeale and Torbett[14] observed a significant backward beamshift. We must therefore conclude that the Fourier method is unable to describe the diffraction experiments of Ref. 14.

F. Results for bounded beams using the inhomogeneous waves decomposition

Figure 9 shows the theoretical result for 2 MHz, $\theta^{inc} = 22.59°$, and a physical beamwidth of approximately 1 cm. No beamshift is seen. Figure 10 shows the same result, but now for a frequency of 6 MHz. Clearly, a beamshift Δ is observable. Figs. 9 and 10 correspond so well to what Breazeale and Torbett[14] have observed, that they are almost exact copies of their pictures.[14]

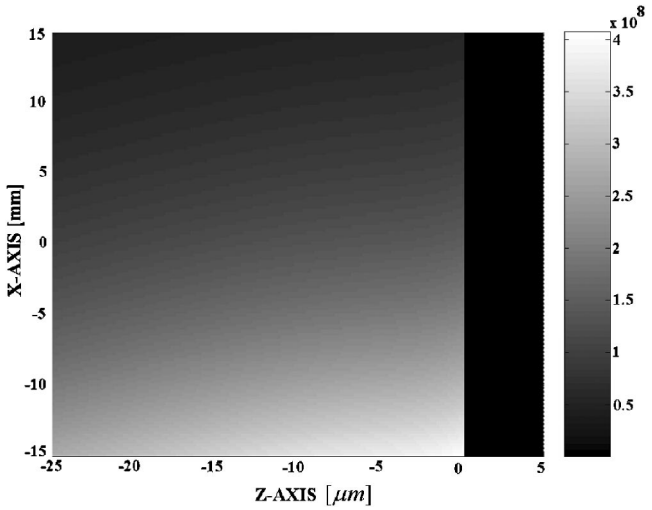

FIG. 6. Amplitude of the *z* displacement as a function of depth and propagation. Same physical circumstances as in Fig. 4. Due to energy leakage, the amplitude drops while propagating.

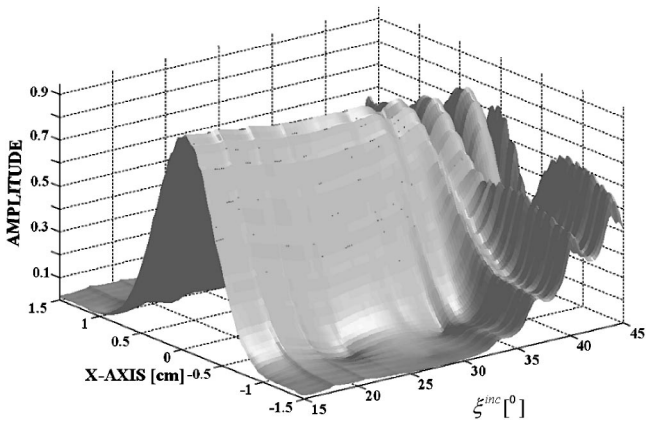

FIG. 8. Same legend as in Fig. 7, except that a physical beamwidth of 1 cm is used. Hence, one would expect to find what Breazeale and Torbett have experimentally observed, which is certainly not the case.

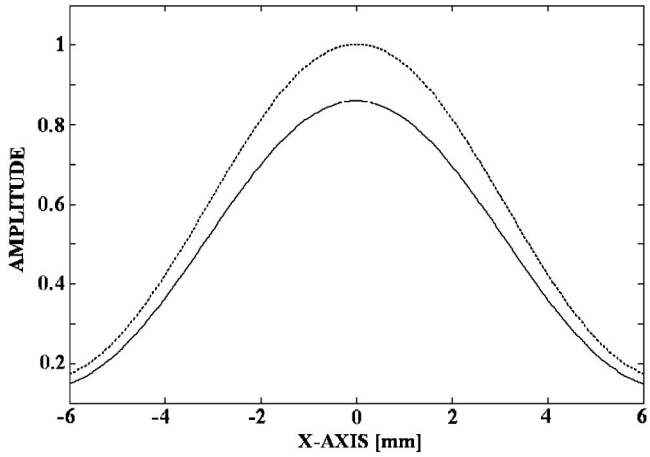

FIG. 9. Here, the inhomogeneous wave theory is used. The incident (dotted line) and the reflected (solid line) beam profile at a frequency of 2 MHz and an angle of incidence of 22.59°. No displacement is observed, which is in agreement with the experiments of Breazeale and Torbett.

If the same incident beam is used, as in Fig. 10, but now at $\theta^{inc}=43.07°$, Fig. 11 is obtained. At $\theta^{inc}=44.63°$, Fig. 12 is obtained. It is seen that Figs. 11 and 12 also show no beamshift (Fig. 11) or an almost negligible forward beamshift (Fig. 12). This is also in agreement with the observations in Ref. 14, where no significant beamshift beyond 40° is found. It is important to remark that, the narrower a bounded beam, the higher the inhomogeneities needed in the decomposition (42). Because the peaks and valleys in Fig. 3 appear at larger inhomogeneities than in Fig. 2, it can be expected that a narrower bounded beam is better influenced by those peaks and valleys and can therefore show displacements (forward or backward). In other words, the narrower the incident beam, the more likely a beamshift may occur in the angle interval of 40°–45°.

VI. CONCLUDING REMARKS

This paper has proved that the inhomogeneous wave theory is capable of elucidating the backward beamshift that has been observed by Breazeale and Torbett[14] and, besides a short demonstration[27] of the capability of the inhomogeneous wave theory to simulate the phenomenon, has been unexplained ever since. It is found that this effect is caused by the interaction of a leaky Scholte-Stoneley wave with other diffracted waves. This is a new phenomenon and was first theoretically proved,[28] shortly before its experimental discovery.[29] Also, it is shown how a bounded beam, narrower than the one in the original experiments of Breazeale and Torbett,[14] is predictable to show the expected backward or forward displacement, unlike the cited experiments. Furthermore, a better insight is given in the nature of the Wood anomalies in diffraction spectra. Therefore, even though the described diffraction theory has also been proved to be very valuable in architectural acoustics,[30] perhaps one of the most beautiful phenomena it has ever explained is the one described in the current paper.

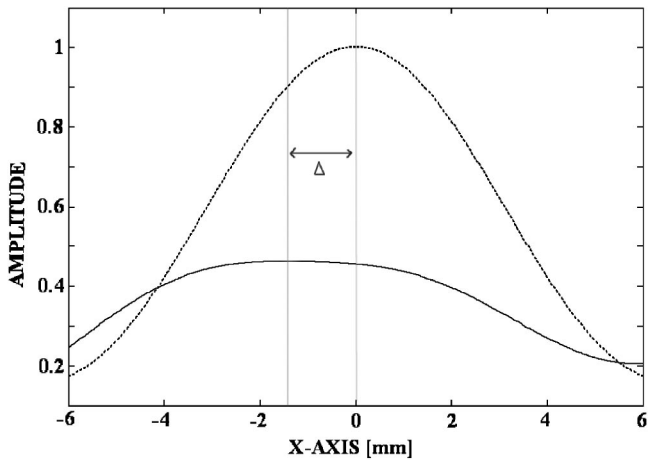

FIG. 10. Same situation as in Fig. 9, except that the frequency is now 6 MHz. A backward beamshift is observed, which is in agreement with the experiments of Breazeale and Torbett.

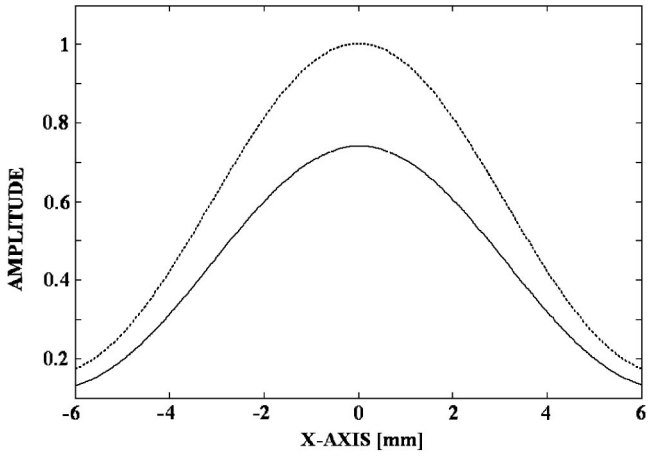

FIG. 11. Same legend as in Fig. 10, except that the angle of incidence here is 43.07°, which is the angle at which the zero-order reflection coefficient shows a maximum. (see Fig. 3). No displacement is observed, which is in agreement with the experiments of Breazeale and Torbett.

ACKNOWLEDGMENTS

The authors wish to express their gratitude to "The Flemish Institute for the Encouragement of the Scientific and Technological Research in Industry (I.W.T.)" for sponsoring.

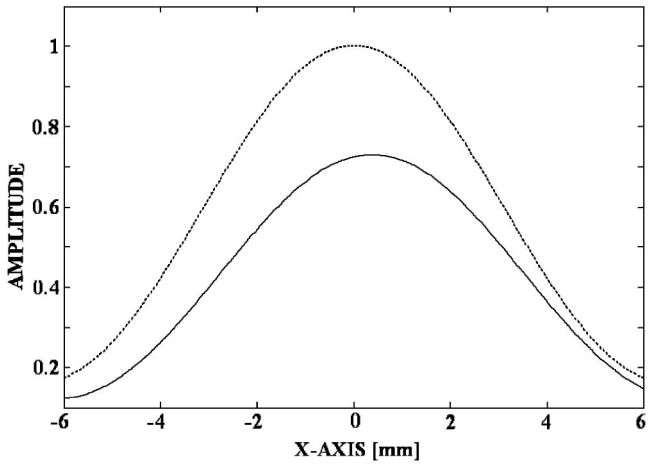

FIG. 12. Same legend as in Fig. 11, except that the angle of incidence here is 44.63°, which is the angle at which the −1-order reflection coefficient shows a maximum (see Fig. 3). Only a negligible displacement is observed, which is in agreement with the experiments of Breazeale and Torbett.

[1]D. Maystre, *Selected Papers on Diffraction Gratings*, SPIE Milestone Series Vol. MS 83(SPIE, Washington, DC, 1993).
[2]R. Briers, Ph.D. thesis, KULeuven University, 1995.
[3]R. Briers, O. Leroy, O. Poncelet, and M. Deschamps, J. Acoust. Soc. Am. **106**, 682 (1999).
[4]J.-M. Claeys and O. Leroy, Revue du Cethedec **72**, 183 (1982).
[5]J. M. Claeys, O. Leroy, A. Jungman, and L. Adler, J. Appl. Phys. **54**, 5657 (1983).
[6]B. A. Lippmann, J. Opt. Soc. Am. **43**, 408 (1953).
[7]A. Jungman, O. Leroy, G. Quentin, and K. Mampaert, J. Appl. Phys. **63**, 4860 (1988).
[8]K. Mampaert and O. Leroy, J. Acoust. Soc. Am. **83**, 1390 (1988).
[9]K. Mampaert, P. B. Nagy, O. Leroy, L. Adler, A. Jungman, and G. Quentin, J. Acoust. Soc. Am. **86**, 429 (1989).
[10]N. F. Declercq, R. Briers, O. Leroy, Ultrasonics **40**, 345 (2002).
[11]M. Deschamps, C.L. Cheng, Ultrasonics **27**, 308 (1989).
[12]R. Briers and O. Leroy, J. Phys. IV **C1**(2), 679-682 (1992).
[13]R. Briers and O. Leroy, Reflection of inhomogeneous plane ultrasonic waves on periodically rough solid-vacuum interfaces, Proceedings of International Society for Optical Engineerings, Gdansk-Jurata, Poland, 1992, Vol. 1844, pp. 196–205.
[14]M.A. Breazeale and M. Torbett, Appl. Phys. Lett. **29**, 456 (1976).
[15]M. Deschamps, J. Acoust. Soc. Am. **96**, 2841 (1994).
[16]T. Tamir and H.L. Bertoni, J. Opt. Soc. Am. **61**, 1397 (1971).
[17]B. Poirée, J. Acoust. **2**, 205 (1989).
[18]J. P. Charlier and F. Crowet, J. Acoust. Soc. Am. **79**, 895 (1986).
[19]M. Abramowitz and I. A. Stegun, *Handbook of mathematical functions* (Dover Publications, New York, 1972).
[20]J.-M. Claeys, Ph.D. thesis, KULeuven University, 1985.
[21]O. Leroy, *Acoustic Interaction with Submerged Elastic Structures*, Series on Stability, Vibration and Control of Systems Series B: Vol. 5, edited by A. Guran, J. Ripoche, and F. Ziegler (World Scientific, Singapore, 1996), Pt. I, pp. 129–163.
[22]J. M. Claeys and O. Leroy, J. Acoust. Soc. Am. **72**, 585 (1982).
[23]K. Van Den Abeele and O. Leroy, J. Acoust. Soc. Am. **93**, 2688 (1993).
[24]F.R. Spitzenogle and A.H. Quazi, J. Acoust. Soc. Am. **47**, 1150 (1970).
[25]N.F. Declercq, R. Briers, J. Degrieck, and O. Leroy, IEEE Trans. Ultrason. Ferroelectr. Freq. Control **49**, 1516 (2002).
[26]K.E.-A. Van Den Abeele, R. Briers, and O. Leroy, J. Acoust. Soc. Am. **99**, 2883 (1996).
[27]N.F. Declercq, J. Degrieck, R. Briers, and O. Leroy, Appl. Phys. Lett. **82**, 2533 (2003).
[28]N.F. Declercq, J. Degrieck, R. Briers, and O. Leroy, J. Acoust. Soc. Am. **112**, 2414 (2002).
[29]A. A. Teklu and M. A. Breazeale, J. Acoust. Soc. Am. **113**, 2283 (2003).
[30]N.F. Declercq, J. Degrieck, R. Briers, and O. Leroy, J. Acoust. Soc. Am. (to be published).